




Indicators of suspended sediment transport dynamics in rivers

Jae hun Shin , Robert C. Grabowski * and Ian Holman 

School of Water, Energy and Environment, Cranfield University, College Road, Cranfield MK43 0AL, UK

*Corresponding author. E-mail: r.c.grabowski@cranfield.ac.uk

 J huns, 0000-0002-2606-0568; RCG, 0000-0002-0926-1202; IH, 0000-0002-5263-7746

ABSTRACT

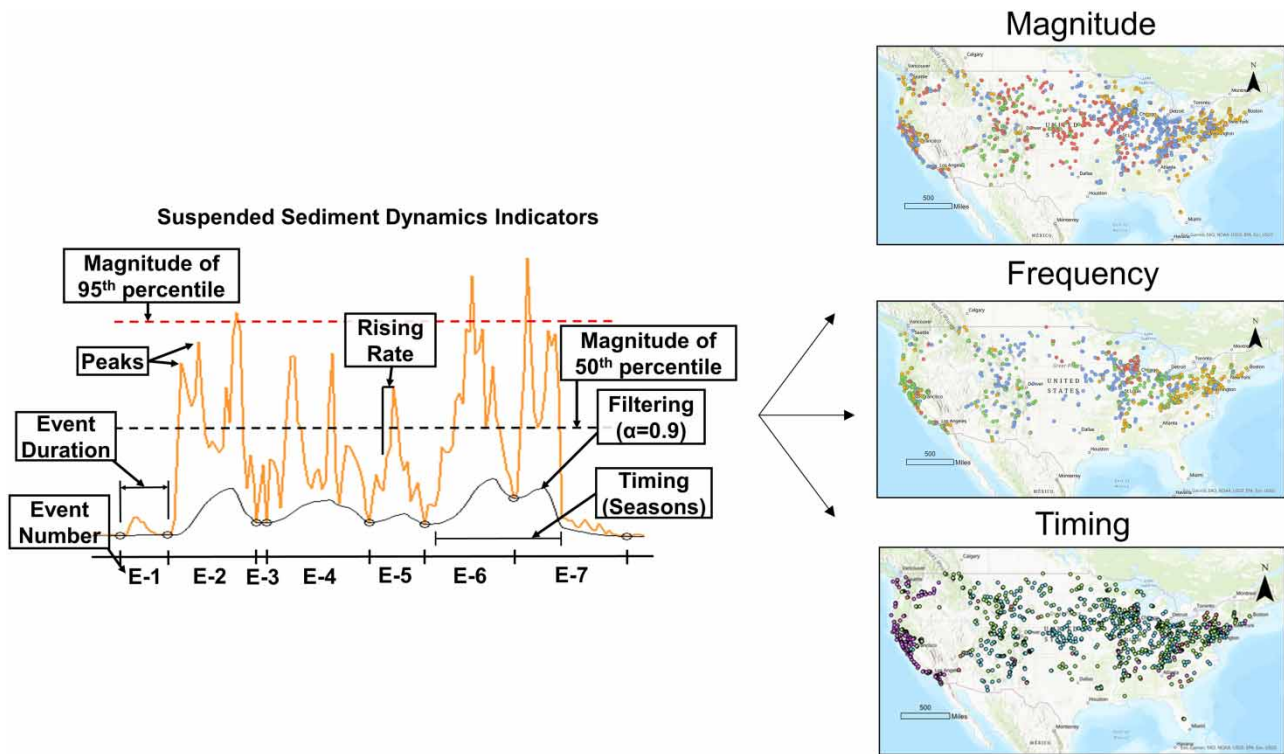
Suspended sediment (SS) is a natural component of rivers, but elevated SS concentrations (SSCs) can impact aquatic ecosystems and engineering infrastructures. However, a significant gap remains in predicting SSC dynamics, which are influenced by catchment and climate factors that control sediment erosion, transport and deposition. The research aim is to develop and apply new SS transport dynamics indicators to determine how SSC varies spatially and temporally at a continental scale. Daily SSC data (mg/l) from 1,425 gauging stations in the US were used to calculate indicators of magnitude, frequency and timing (MFT). A filtering approach was applied to calculate frequency indicators that capture SSC events of differing durations. Spatial patterns in indicators were examined and integrated using K-means clustering. High SSC was identified at sites in dry and mountainous regions, but longer-duration SSC events were found in the northern US. The western coastal region and Puerto Rico had consistent timings of high SSC (winter and autumn, respectively). SSC magnitude had a decreasing trend over time across most of the US, but increasing trends were identified for the duration of SSC events. The use of MFT indicators is recommended for future studies to support prediction of climate change impacts on SSC.

Key words: box statistics, conterminous US, Magnitude, Frequency and Timing (MFT), K-means clustering, magnitude, suspended sediment dynamics indicators

HIGHLIGHTS

- Short-term variations in suspended sediment concentrations (SSCs) in rivers studied with new indicators.
- High-magnitude SSC was found in mountainous and dry regions and longer SSC events in the Upper Midwest.
- An increasing trend in the duration of SSC events was found, despite decreasing SSC magnitude.
- M95, rising rate, and duration and timing of SSC events ($\alpha = 0.6$) are recommended as indicators for future studies.

GRAPHICAL ABSTRACT



INTRODUCTION

Suspended sediment (SS) is an important part of river systems but is challenging to manage due to the high variability in SS transport dynamics (Cohen *et al.* 2022), caused by a wide range of climate and catchment factors (Vercruyssen *et al.* 2017). SS concentrations and their temporal dynamics affect aquatic ecological communities and the geomorphic evolution of river systems (Bilotta & Brazier 2008; Neachell 2014; Wharton *et al.* 2017; Poepl *et al.* 2019) and influence decision-making for water resources management, such as the control of intakes for water abstraction and hydropower operations to prevent SS inflows into the systems (Tsyplov *et al.* 2021). With decadal trends in SS flux and increased uncertainties with climate change (Moragoda & Cohen 2020), a deeper understanding of SS transport dynamics is needed.

SS transport dynamics studies focus typically on the calculation and analysis of sediment load, which is the mass of sediment transported per unit time (month or year) based on SS concentration and discharge data (Roman *et al.* 2012; Yilmaz *et al.* 2018). Sediment load is useful for calculation of total flux of SS, and in conjunction with the hysteresis in SS rating curves, it can be related to catchment hydrological and geomorphic processes (Horowitz 2003; Misset *et al.* 2019). Studies on sediment load have identified the relative impacts of factors operating at different spatial and temporal scales, such as different vegetation cover and erosion factors, e.g. gullies (Vercruyssen *et al.* 2017), and relationships between the two main drivers of SS transport, discharge and rainfall (Khan *et al.* 2016; Kemper *et al.* 2019). However, it remains difficult to identify the spatio-temporal patterns in, and drivers of, shorter time scales of transport dynamics (days to months) due to the paucity of data.

Most SS transport studies use data from a single temporal scale, often with substantial spatial and temporal gaps, which limits our understanding of drivers (Francke *et al.* 2014; Vercruyssen *et al.* 2017). A recent study has helped to address this challenge through a multi-scale analysis of the variability in the rating curve relationship between SS transport and river discharge, using turbidity as a surrogate (Wang & Steinschneider 2022). The approach allowed the identification of catchment characteristics that affect the stability of turbidity-discharge relationships, such as stream network complexity, perennial snow coverage, and saturation-excess overland flow. The incorporation of transport dynamic indicators into these multi-scale

analyses, i.e. magnitude, frequency and timing (MFT) of events, as is done for other areas of hydrology and water quality, has the potential to further specify the contribution of different factors to SS transport dynamics (Mize *et al.* 2018; Misset *et al.* 2019).

An MFT approach has the potential to generate a richer representation of temporal variability of SS transport, which can be combined with analytical approaches, like multivariate data mining techniques, to relate to underlying environmental or human factors (Vercruyse *et al.* 2017). Magnitude indicators, especially those that capture extreme values, like 95th percentile, are useful to link with extreme values of precipitation, especially flows and sediment yield (Stryker *et al.* 2018; Whitfield & Shook 2020). Indicators of frequency relate to both the number of events per unit of time and the duration of those events, which can help to identify the underlying factors affecting the hydrological responsiveness of the catchment and sediment generation and transport mechanisms. For example, long-duration SSC events can indicate large catchments and large weather-related drivers, such as hurricanes or monsoons, while short events can relate to convective storms that might be frequent (continental climate) or infrequent (arid climate) (Alexandrov *et al.* 2007; Yao *et al.* 2022). The timing of high SSC can be influenced by factors such as climate or land use that influence the generation, mobilization and delivery of SS (Rose & Karwan 2021). These underlying factors can be better understood when a hierarchy of temporal scales and frequency is considered. Previous research has used monthly (Girolamo *et al.* 2015) and event-based scales (Nosrati *et al.* 2021) to investigate sediment transport dynamics within watersheds (Kemper *et al.* 2019).

The study aim is to use an MFT approach to determine the spatial patterns and temporal trends in short-term (daily to monthly) SS transport dynamics that exist at a continental scale. The objectives of the study are to (i) develop and evaluate new indicators of SS dynamics based on MFT, (ii) determine how the new indicators are distributed across the continent and identify spatial patterns and heterogeneity, and (iii) evaluate the indicators to provide recommendations for future studies. Spatial patterns in SS indicators could provide insights into catchment and climate controls on SS generation and transport that could inform environmental water management practices.

STUDY AREA AND DATA

The study area was the contiguous US and the islands of Hawaii and Puerto Rico, which has a diversity of climates, landscapes, and land use and land cover (LULC) (Liu *et al.* 2020) that could influence sediment transport regimes and SSC dynamics. The US Geological Survey (USGS) provides daily SSC data at 1,667 monitoring sites on rivers, including in overseas territories. A text file format of the SSC data (Parameter code: 80154) was obtained from USGS (U.S. Geological Survey 2016) (Figure 1). This dataset is described as 'sediment, suspended (milligrams per litre)' and is derived from instantaneous SS concentration collected from water samples using an approved sampling method (Edward & Douglas Glysson 1999), interpolated and flow-weighted to estimate a mean daily SSC for the monitored point (river cross-section; Porterfield 1972; Sommerfield 2016).

Filtering and processing were kept to a minimum to retain the greatest number of sites to investigate spatial patterns in SSC. Sites were selected that had greater than 365 days of record and a minimum of 200 days of SSC data. In total 1,425 sites were selected with an average record length of 9 years (min = 1 year, max = 80 years) and SSC data covering an average of 83.6% of days per site and period of record (min = 6.2% and max = 100% of available daily data). Please see the supplementary material for more information on the sites, catchment areas, and length and completion of SSC records (Figure A-1).

Previous research identified limitations in USGS SSC data that can affect annual SS load calculations (Sommerfield 2016), which has led some researchers to use turbidity as a proxy for SSC (Wang & Steinschneider 2022). A strong correlation was observed between SSC and turbidity, with coherence in the timing and duration of SSC events, for a subset of these sites, which were selected for further analysis in a study on catchment and climate drivers (Shin *et al.* In Revision). Those correlations provided confidence in the use of the SSC data to develop and test the indicators, with the large number of SSC sites providing greater coverage to explore potential spatial patterns in SSC transport dynamics.

METHODS

The methodology comprised several steps: (i) developing MFT indicators that characterise short-term variations in daily SSC; (ii) evaluating covariation in the MFT indicators using multivariate approaches (Principal Component Analysis, PCA) to reduce the number of indicators; (iii) visualising the spatial patterns in MFT indicators; and (iv) analysing their spatial variability using spatial statistics, clustering and temporal trends using trend analysis.

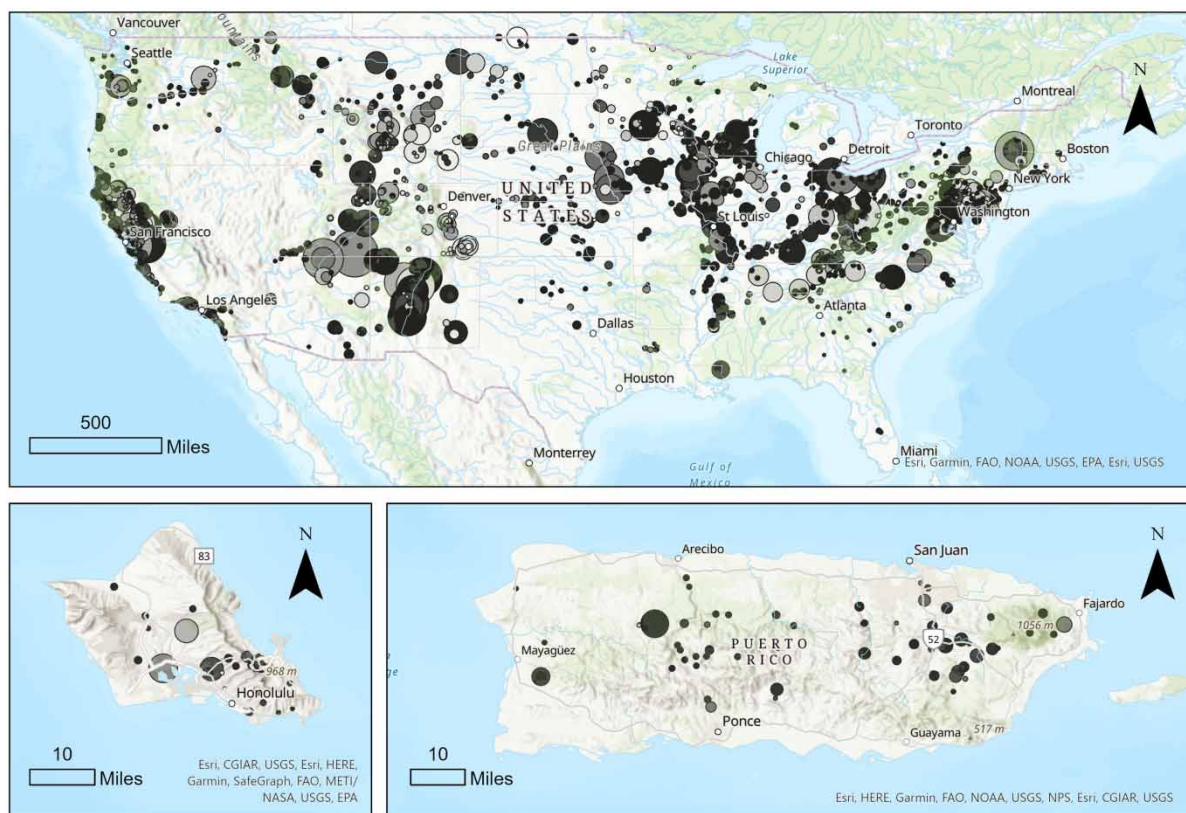


Figure 1 | Locations and quality of daily mean SSC from USGS gauging stations: Symbol sizes are proportional to the duration of monitoring record (min – 1 year, max – 80 years). Colour indicates completeness of the monitoring records (min – 6.2%, max – 100%): darker colour represents greater data completeness. Top: continental US (1,329 sites), bottom left: Honolulu, Hawaii (35 sites), bottom right: Puerto Rico (61 sites).

Indicators to describe SS dynamics

Indicators to describe SSC dynamics were developed on an average annual basis to capture variation in the MFT of SS transport (Table 1 and Figure 2). All indicators were computed annually, and the annual time series was collapsed to a single indicator for each site. Calculation of indicators was conducted in RStudio based on daily mean SSC (Posit team 2022).

Magnitude indicators

Magnitude indicators were developed to capture intra- and inter-annual changes in SSC (Figure 2). Average annual values were calculated for each indicator in each water year (Oct–Sep). The magnitude of different percentiles (95th, 75th, 50th and 25th) was calculated for each year of record and averaged across the number of years per record (M95, M75, M50, M25). Rising and falling rates (i.e. positive and negative changes in SSC per day, respectively) were calculated by subtracting the previous day values from current day values, as the time series consisted of daily data, and then averaged across the period of record (rising rate – R.r., falling rate – F.r.). Peaks in the SSC record were identified from the rising/falling rate time series by detecting positive to negative inflection points, with a maximum peak duration set at 7 days (Yu & Disse 2017). The number of peaks per year was calculated and then averaged across the number of years per record. The date of each peak was exported for use as a timing indicator, more information is given in the following. Finally, the standard deviation of monthly minimum and maximum values was calculated (Sd.min and Sd.max, respectively).

Frequency indicators

Frequency indicators were developed to capture event-based SS transport dynamics: the duration of a high SSC event (event duration), the number of SSC events per year (event count) and the number of SSC peaks within an event (peaks per event

Table 1 | Indicators to describe temporal variations in SSC (daily mean) based on MFT

Symbols	Indicators	Description	
Magnitude	M95	95th percentile	Avg. annual 95th percentiles of SSC
	M75	75th percentile	Avg. annual 75th percentiles of SSC
	M50	50th percentile	Avg. annual 50th percentiles of SSC
	M25	25th percentile	Avg. annual 25th percentiles of SSC
	R.r.	Rising rates	Avg. annual daily increase in SSC
	F.r.	Falling rates	Avg. annual daily decrease in SSC
	Stdev.max	Standard deviation of monthly max values	Avg. annual values of standard deviation of monthly maximum SSC
	Stdev.min	Standard deviation of monthly min values	Avg. annual values of standard deviation of monthly min SSC
Frequency	D	Duration of events	Avg. annual duration of SSC events, in days, for four different frequencies (α)
	C.of.e.	Count of events	Avg. annual number of SSC events for four different frequencies (α)
	P.p.e.	Number of peaks per event	Avg. annual number of peaks per SSC event for four different frequencies (α)
Timing	Month.max.sum	Month of max total SSC	Month with the maximum total SSC, summed across the time series of record
	Month.i.p.max	Month of max number of inflection points	Month with the maximum number of events, defined as inflection points in the SSC timeseries

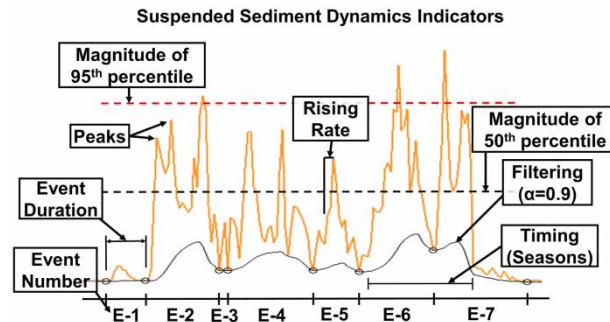


Figure 2 | Indicators of SS dynamics in rivers were developed based on the MFT of changes in SS concentration.

(P.p.e.) (Figure 2). The ‘baseflows’ package in R was used to identify where daily SSC values in a time series deviate over time, in a process akin to baseflow separation for river flows (Ladson *et al.* 2013). The analysis draws filtering (e.g. baseflow) curves with Lyne and Hollick’s filter (Equations (1) and (2)) and identifies contact points in the SSC data, where the SSC timeseries data make contact with and then separate from the curve.

$$c_f(i) = \begin{cases} \alpha c_f(i-1) + \frac{(1+\alpha)}{2} [c(i) - c(i-1)] & \text{for } c_f(i) > 0 \\ 0 & \text{otherwise} \end{cases} \quad (1)$$

$$c_b(i) = c(i) - c_f(i) \quad (2)$$

where $c_f(i)$ is a peak at the i th sampling. $c(i)$ is the original concentration at the i th sampling. $c_b(i)$ is the baseline at the i th sampling. α is the filter parameter controlling the shape of the baseflow line.

Four α values (0.975, 0.9, 0.6, 0.2) were used to capture SSC events lasting a range of durations, from months to days (see the results section for an example). A value of 30 days was used for the parameter 'n.reflected', based on initial testing and previous studies (Ladson *et al.* 2015). While the filtering process worked well overall, it encountered problems when applied to the longest frequencies due to the presence of data gaps in some sites. Consequently, frequency indicator values were not able to be calculated for the 0.975 and 0.9 α values at 29 and 6 of the 1,425 sites, respectively.

The event duration was calculated based on the contact points identified in the 'baseflow' filtering, i.e. the dates when the SSC data and filtering curves had the same value, subtracting the end date from the start date. The analysis was conducted for all four α values (D0.975, D0.9, D0.6, D0.2). As α values become smaller, the filtering curves plot closer to the SSC curve, and short-duration events are identified. The number of events per year was counted and then averaged across the number of years per record (count of events – C.of.e.). The analysis was conducted for all four α values (C.of.e0.975, C.of.e0.9, C.of.e0.6, C.of.e0.2). Finally, SSC peaks that occurred during an SSC event were counted, as described above in the magnitude indicators (P.p.e.). The analysis was conducted for all four α values (P.p.e0.975, P.p.e0.9, P.p.e0.6, P.p.e0.2). Duration and counts were recorded at the event end dates and averaged across the number of years.

Timing indicators

Two indicators of the timing of high SSC were developed and calculated, relating to magnitude and frequency (Figure 2). First, the month with the highest SSC (i.e. magnitude) was identified by totalling the daily SSC values for each month across the time series of records at 1,425 sites. Second, the month with the highest number of SSC peaks (i.e. frequency) was determined by totalling the number of contact points (i.e. inflection points at local minima where SSC data and the filtering curves have the same value for the date), as described in the frequency section above, for different α values (0.975, 0.9, 0.6, 0.2) for each month across the timeseries of record. Sites having the same monthly values in different seasons were removed in the end to avoid selecting median month value ($\alpha = 0.975$, 1,008 sites; $\alpha = 0.9$, 1,085 sites; $\alpha = 0.6$, 1,213 sites, $\alpha = 0.2 = 1,248$ sites). The results were aggregated and reported based on the season: winter – December, January & February (DJF); spring – March, April, May (MAM); summer – June, July and August (JJA); and autumn – September, October and November (SON).

Data analysis

Principal component analysis

A PCA was conducted with the SS transport dynamics indicators using 'factoextra' package in R as an initial data simplification step (Hegde 2016). Indicators were selected for further analyses based on being associated with different axes to remove indicators with high degrees of covariation. Following removal of sites with gaps in indicators, a total of 1,364 sites were included in the analysis.

Trend analysis

A Mann–Kendall trend analysis from R package 'Kendall' was used to detect trends in all average annual magnitude and frequency indicators, for each site (Kar & Sarkar 2021). Sites with significant trends (p value < 0.05) were identified and selected for visualization and discussion.

Block statistics

Large-scale spatial patterns in the SS indicators across the study area were visualised with block statistics in Arc GIS 3.1.0 (Yang *et al.* 2021). Raster files were created for each indicator based on the location of each monitoring station (cell size: 0.087 radian). The coarse resolution raster output had an average of 1.17 sites per cell (min: 1 and max: 7). The outputs of the block statistics were mean and standard deviation of indicators summarised over a larger area (20 × 20 cells, rectangle), resulting in a coarser-resolution raster. Block statistics were not conducted on the sites with statistically significant trends, due to the low point density.

Clustering analysis

K-means cluster analysis was used to integrate the findings across the indicators to find general patterns that might relate to natural and anthropogenic factors (Plexida *et al.* 2014; Celestino *et al.* 2018; Fang *et al.* 2021). K-means clustering was conducted in ArcGIS Pro 3.1.0 using the multivariate clustering function. Magnitude and frequency indicators were log-transformed (Tomlinson *et al.* 2018), and timing indicators were left untransformed. The number of clusters was informed by Elbow and Silhouette methods (Masud *et al.* 2018), with a final decision based on interpretability (Ballabio *et al.* 2017).

RESULTS

PCA

The PCA identified considerable covariance between SS transport dynamic indicators, suggesting that a reduced number of indicators could be used for visualization and analysis (Figure 3). Magnitude indicators were aligned with PCA axis 1, which explained 29.5% of the variance in the dataset. The strongest positive scores related to M95, M75 and rising rate (R.r.), while the only negative score was falling rate (F.r.), which was opposite to R.r. Frequency indicators were aligned closely with PCA axis 2, which explained 22.3% of the variance in the data. Generally, the number of events (C.of.e.) had positive scores, while P.p.e. and event duration (D) were negative. From this analysis, a selection of magnitude, duration and P.p.e. indicators were taken forward in the analysis, subselecting those that occupy different dimensions of the PCA plots (M95, M25, D0.9, D0.6, P.p.e. 0.6). Note: C.of.e. indicators were not taken forward as there was little differentiation between these vectors, and indicators with $\alpha = 0.975$ were not used due to the previously mentioned issue with calculation of the indicators when there were gaps in SSC record.

Block statistics

Magnitude indicators

Spatial patterns of extreme high and low SSC were evident from the magnitude indicators (Figure 4). Both M95 and M25 had similar spatial patterns across the continental US, with generally low values across most of the US, but with higher SSC in the driest regions of the country and a single location in the Eastern Temperate Forest ecoregion, around Atlanta, Georgia (Figure 4(a) and 4(c)). The highest extreme SSC values (M95) were found in the Rocky Mountains, Great Plains and southern

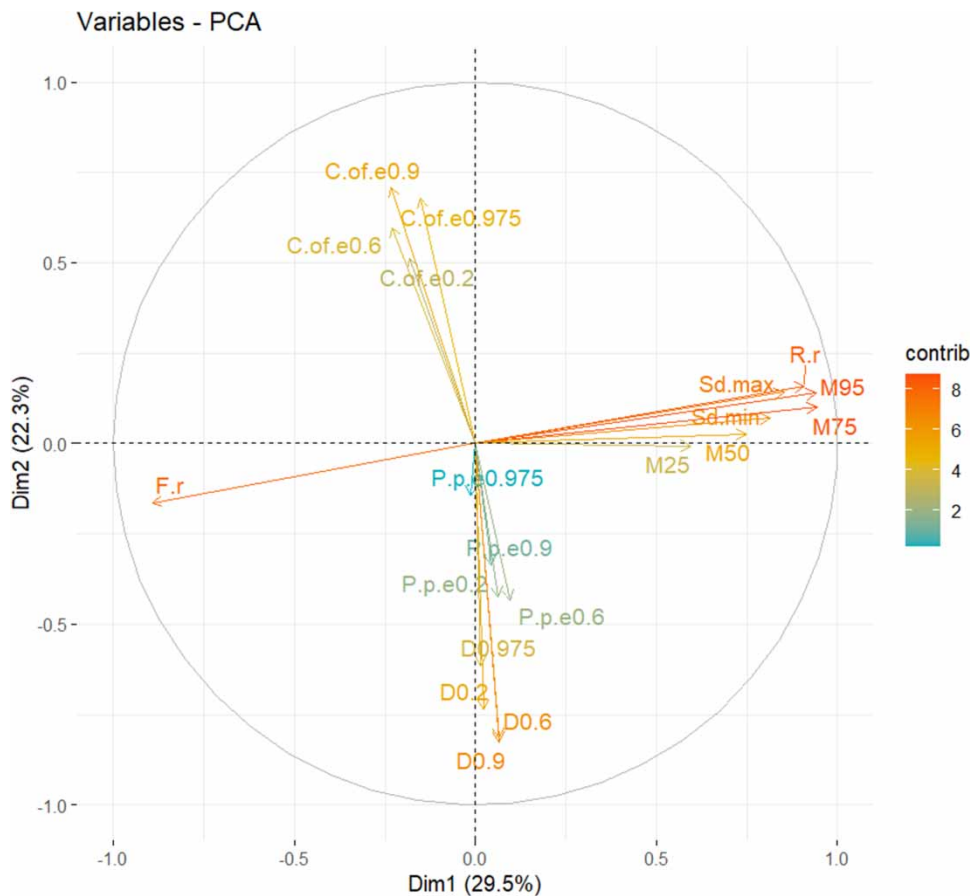


Figure 3 | PCA result of magnitude and frequency indicators for the mean annual indicators. Magnitude: M95, M75, M50 and M25 – daily SSC at different percentiles; R.r. – rising rate; F.r. – falling rate; Sd.max and Sd.min – standard deviation of monthly max and min values. Frequency: D – duration of events; C.of.e. – count of events; P.p.e. – Peaks per event. 'contrib': Contributions of variables. Please refer to the online version of this paper to see this figure in colour: <http://dx.doi.org/10.2166/nh.2023.068>.

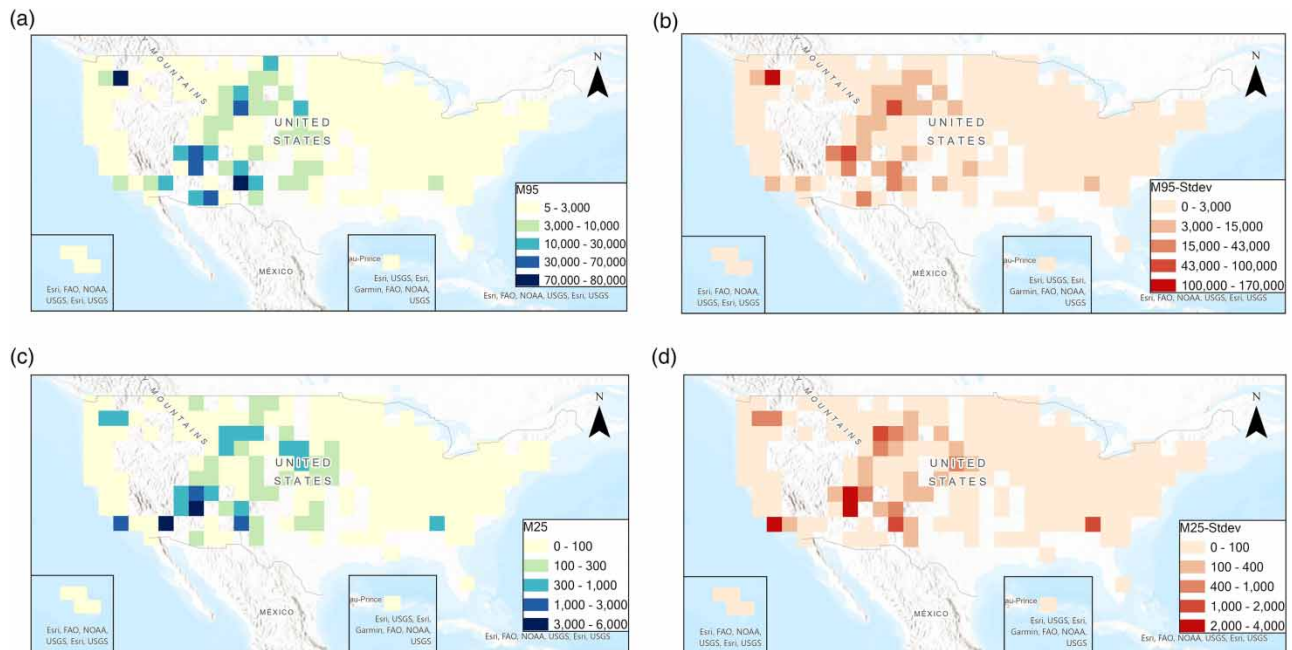


Figure 4 | Spatial distribution of M95 and M25 including standard deviation: M95 and M25 represent magnitude of 95th and 25th percentiles (a and c), respectively. Stdev is standard deviation (b and d). Please refer to the online version of this paper to see this figure in colour: <http://dx.doi.org/10.2166/nh.2023.068>.

deserts (Figure 4(a)). A notable outlier is the extremely high SSC values in the Northwest, which relate to the Mount St. Helens eruption in 1984 (Figure 4(a) and 4(c)). Elevated M25 was found at similar locations as M95. However, some areas, e.g. Rocky Mountains and deserts, had generally lower M25 relative to their high M95; while others, e.g. Great Plains had higher M25 (Figure 4(a) and 4(c)). Standard deviation (Stdev) of magnitude values was generally low across the US and areas of high Stdev were located in areas of high M95 or M25 (Figure 4(b) and 4(d)).

Frequency indicators

The use of multiple α values allowed the calculation of frequency indicators for SSC events occurring across a broad range of temporal scales, with lower α values identifying shorter duration events (Figure 5). The largest α value (0.975) identified the longest duration events, i.e. multi-month (Figure 5(a)), which ranged in length from 1 to 370 days (mean = 57.2) (Figure 5(b)). An α of 0.9 identified events that lasted approximately one month in duration, ranging in length from 1.5 to 86.5 days (mean = 22.3). The smaller α values identified events that lasted a single day to weeks. The duration of events for 0.6 ranged in length from 1 to 57.9 days (mean = 9.56), while for 0.2, it ranged in length from 1 to 55.3 days (mean = 6.3) (Figure 5(b)). As the α value decreased, the C.of.e. increased and number of P.p.e. decreased (Figure 5(c) and 5(d)).

The frequency indicators had different spatial patterns from the magnitude indicators, which also varied by α value (Figure 6). The duration of events at $\alpha = 0.9$ were around 20–30 days for much of the US, with a cluster of longer durations in the upper Midwest and scatter in locations in California, the Northwest, Rocky Mountains and Puerto Rico (Figure 6(a)). Duration of events at $\alpha = 0.6$ showed greater spatial heterogeneity, with a cluster of short durations in the Appalachian region, lasting 8–10 days, and similar locations of long durations, lasting 20–30 days, as for $\alpha = 0.9$. P.p.e. also had high spatial variability, with slightly higher numbers in the inland and overseas territories (Figure 6(e)). Standard deviations were the highest in locations with the highest durations and P.p.e. (Figure 6(b), 6(d), 6(f)).

Timing indicators

Spatial patterns were observed in the SSC timing indicators, though these were more pronounced for magnitude than frequency (Figure 7). The maximum SSC was consistently found in the winter months (DJF) in the West Coast (e.g. California and Washington State; Figure 7(a), purple) and in the autumn (SON) for Puerto Rico (Figure 7(a), red). The

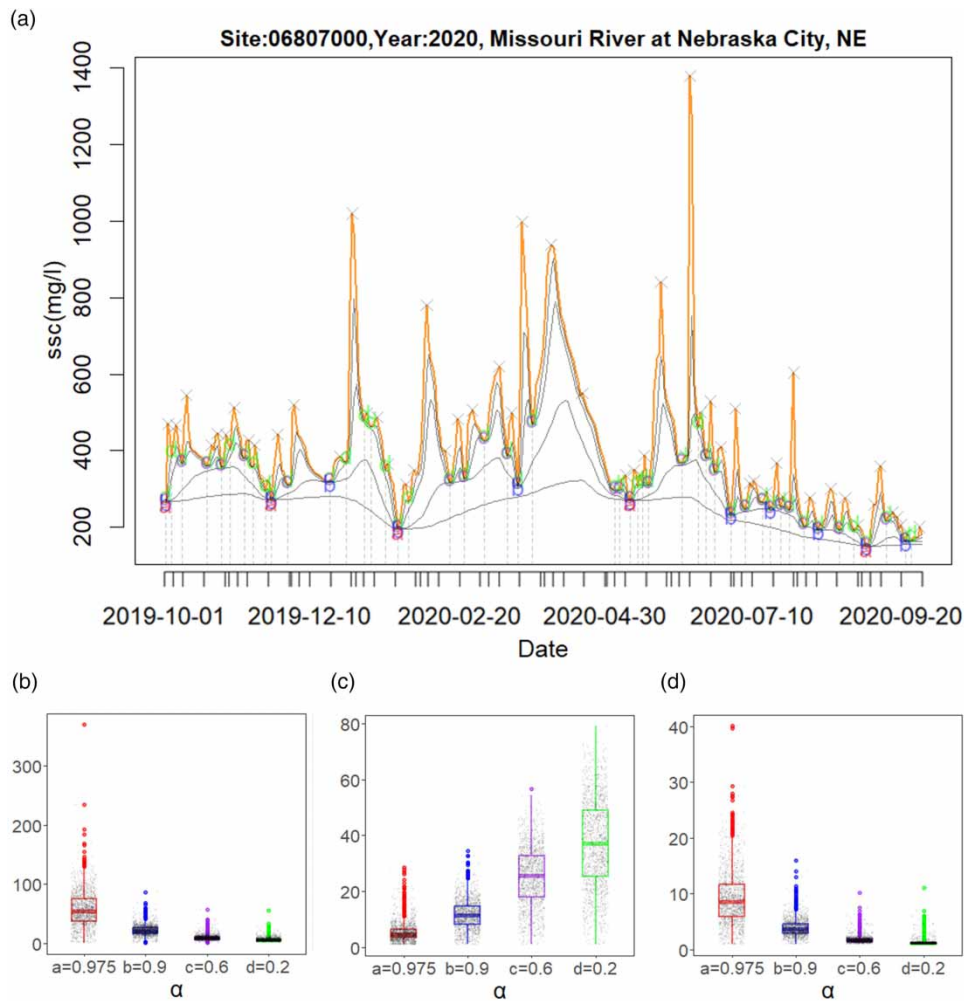


Figure 5 | Impact of α value on the frequency indicators. An example of SSC timeseries (orange) illustrating the length of SSC events at different α (Red = 0.975, Blue = 0.9, Purple = 0.6, Green = 0.2) (a). The start/end of events is located where the filtering curves make contact with the SSC (i.e. pairs of the same letters in the same colours). Duration of event (b). Count of events (c). Peaks per event (d). Please refer to the online version of this paper to see this figure in colour: <http://dx.doi.org/10.2166/nh.2023.068>.

Great Plains and Midwest regions had their greatest SSC in spring and summer (Figure 7(a), green and blue). The season with the highest number of SSC events had greater variability across the US, with no clear spatial patterns ($\alpha = 0.6$; Figure 7(b)). The choice of α value may potentially be important for this indicator; more sites had an autumn (SON) timing with higher α values (e.g. longer duration events), while more sites had a summer (JJA) timing at lower α values (e.g. shorter duration events; Supplementary material, Figures A2 and A3).

Trend analysis

The trend analysis shows a mixture of increasing and decreasing trends (Figure 8). When all sites are included in the analysis, SSC values appear to be increasing over time, without any obvious spatial patterns in the magnitude of the trend (Figure 8(a)) or standard deviation (Figure 8(b)). However, when only statistically significant trends are shown, it becomes clear that there is a generally negative trend in M95 (Figure 8(c)). Event durations show a more mixed distribution with both increasing and decreasing durations for long (i.e. seasonal) and medium-length (i.e. monthly) events, though there is a greater number of sites showing increasing trends in duration for D0.6 than D0.9 (Figure 8(d) and 8(e)). P.p.e 0.6 had a mixture of increasing and decreasing trends (Figure 8(f)).

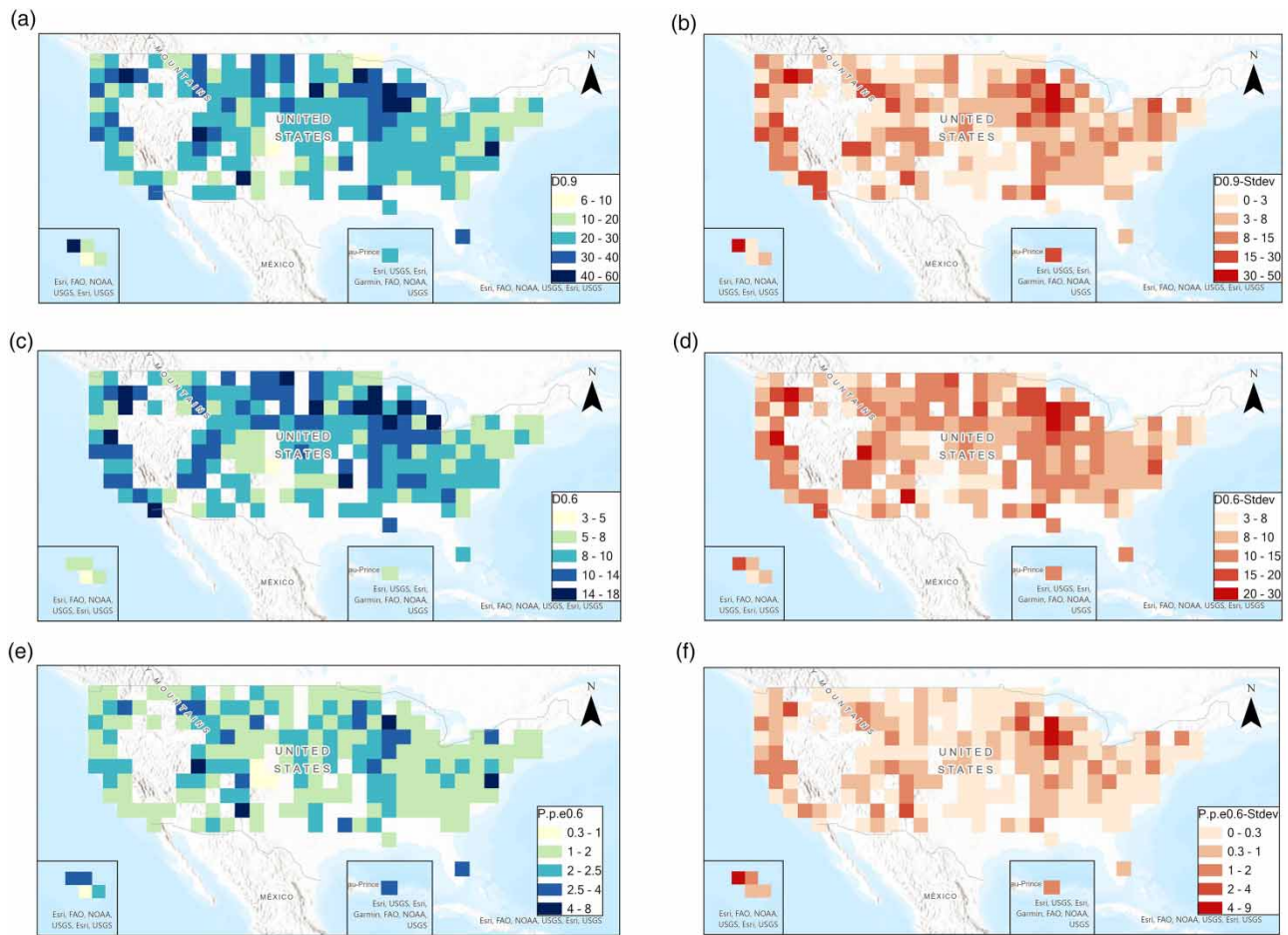


Figure 6 | Spatial distribution of selected frequency indicators and standard deviation: Duration of events at α values of 0.9 (D0.9; a) and 0.6 (D0.6; c); peaks per event at α value of 0.6 (P.p.e.0.6; e). Stdev represents standard deviation (b, d, f). Please refer to the online version of this paper to see this figure in colour: <http://dx.doi.org/10.2166/nh.2023.068>.

Cluster analysis

K-means clustering was conducted using selected MFT indicators. Four clusters were selected based on the results of the Elbow and Silhouette methods, balancing the benefit of a reduction of within sum of squares, but decreasing silhouette width, and the interpretability of the clusters (Supplementary material, Figures A4). The clustering results show clear spatial patterns at the continental scale (Figure 9(a)). A broad cluster of sites with high M50 and R.r. was found distributed across the central US, spanning the Rocky Mountain, desert and Great Plains regions (Figure 9, cluster 4, yellow). Sites with a longer duration of SSC events ($\alpha = 0.6$) were found across the US but appear to be clustered in the Midwest and California (Cluster 2, red), along with the Appalachian region. The timing of the maximum monthly SSC was later in the year for the islands and the eastern US region (cluster 3, green), especially compared to the rest of the inland area, e.g. Midwest and broader Mississippi basin (clusters 1 and 2, blue and red, respectively). For the season with the greatest number of events (max i.p. months), the irregular patterns observed at continental scale (Figure 7(b)) were reflected in the clustering analysis (1,3 and 4, blue, green and yellow, Figure 9).

DISCUSSION

This study analysed timeseries of SSC data from river monitoring stations using newly developed indicators of SS transport dynamics based on MFT. Clear spatial patterns were observed for some indicators and indicator classes, which suggest that these SSC indicators are driven by large-scale factors, such as climate or LULC. Other indicators had more complex, and

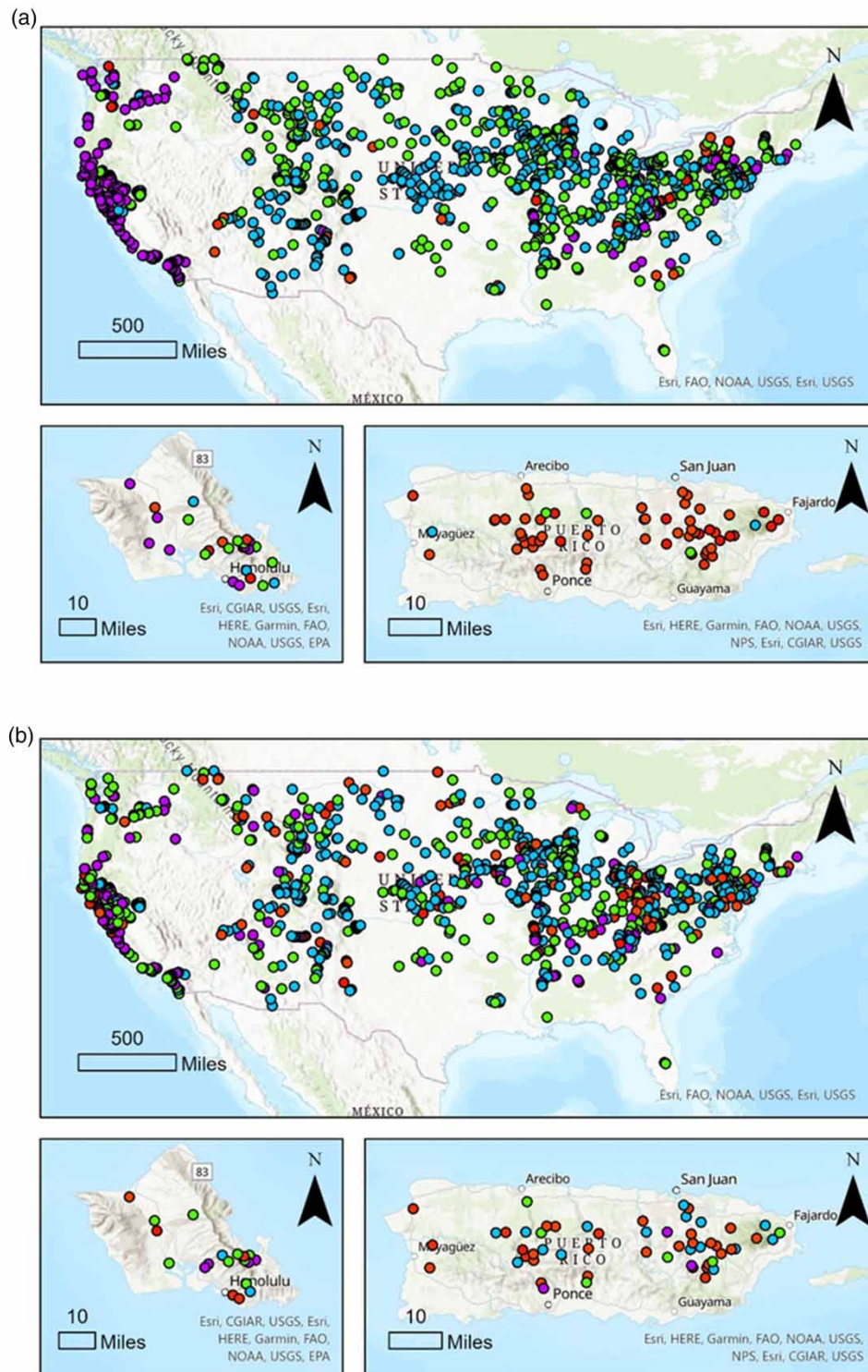
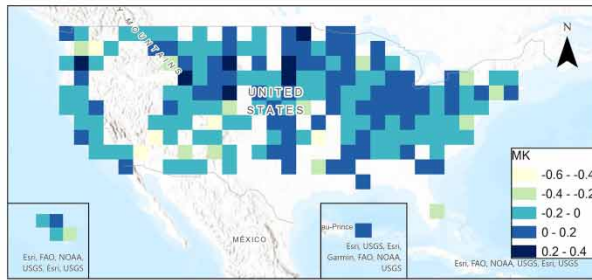


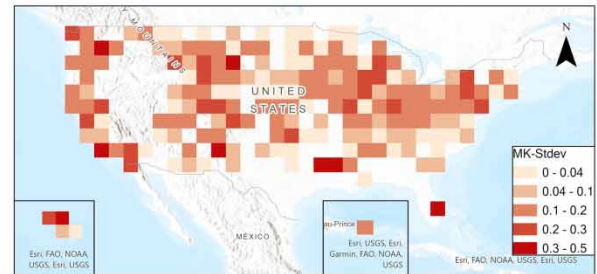
Figure 7 | Seasons with the maximum SSC per month (magnitude; a) and the maximum number of SSC events at α of 0.6 (frequency; b): Winter (DJF) - Purple, Spring (MAM) – Green; Summer (JJA) - Blue; Autumn (SON) – Red. Please refer to the online version of this paper to see this figure in colour: <http://dx.doi.org/10.2166/nh.2023.068>.

heterogeneous spatial distributions, suggest more localised influences in SS transport dynamics. In this section, we summarise these findings on the spatial patterns in SS transport dynamics indicators and make recommendations for their future use in studies to determine the influence of catchment and climate factors.

(a) MK - All time series



(b) MK-Stdev



(c) MK-M95



(d) MK-D0.9



(e) MK-D0.6



(f) MK-P.p.e0.6



Figure 8 | Results of trend analyses: MK means Mann Kendall trend analysis: magnitude of 95th percentiles (M95), duration of events (D), count of events (C.of.e.), and peaks per event (P.p.e.). The Box statistics results (a,b) provide MK trend analysis results from all daily time series. Results of MK trend analysis on the indicator calculation are shown in c,d,e,f, calculated from average annual time series ($p < .05$) with more sediment and blue colours, representing increasing/decreasing trends. Please refer to the online version of this paper to see this figure in colour: <http://dx.doi.org/10.2166/nh.2023.068>.

Of the SSC dynamics indicators, M95 had the most distinctive spatial pattern. M95 and the standard deviation of M95 were low across most of the US (Figure 4). However, elevated values were observed in dry and mountainous regions, especially the Rocky Mountain, North American desert and western Great Plains regions (Li *et al.* 2020a). The high SSC values detected near Mount St. Helens are a clear illustration of the influence of volcanic and other tectonic events on SS transport dynamics, which also impact local ecosystems (Uhrich *et al.* 2021). It highlights the importance of sediment retention systems near possible eruption areas (Hoess & Geist 2021). There was a strong correlation between the magnitude indicators (Figure 3), thus future studies may only require the inclusion of a single magnitude indicator (e.g. M50 or M95), or perhaps a reduced number with slightly different alignment along the PCA axes (e.g. M95 and M25), to investigate climate and catchment controls.

Frequency indicators had continental scale spatial patterns that were distinctly different to magnitude (Figure 6). SSC events were longer in the upper Midwest and lower in the eastern US at all α values (Figure 6(a) and 6(c)). These results could be caused by spatial patterns in climate and precipitation (Akisanola *et al.* 2020). The duration of shorter events (i.e. 1- to 2-week duration) had slightly more defined clusters than long-duration events, especially in the upper Midwest, upper Great Plains and west coast (Figure 6(c)). P.p.e. was generally low across the US, and high values were widely distributed. However, there is a suggestion of a cluster of moderate to high values along the Mississippi River, especially in the upper

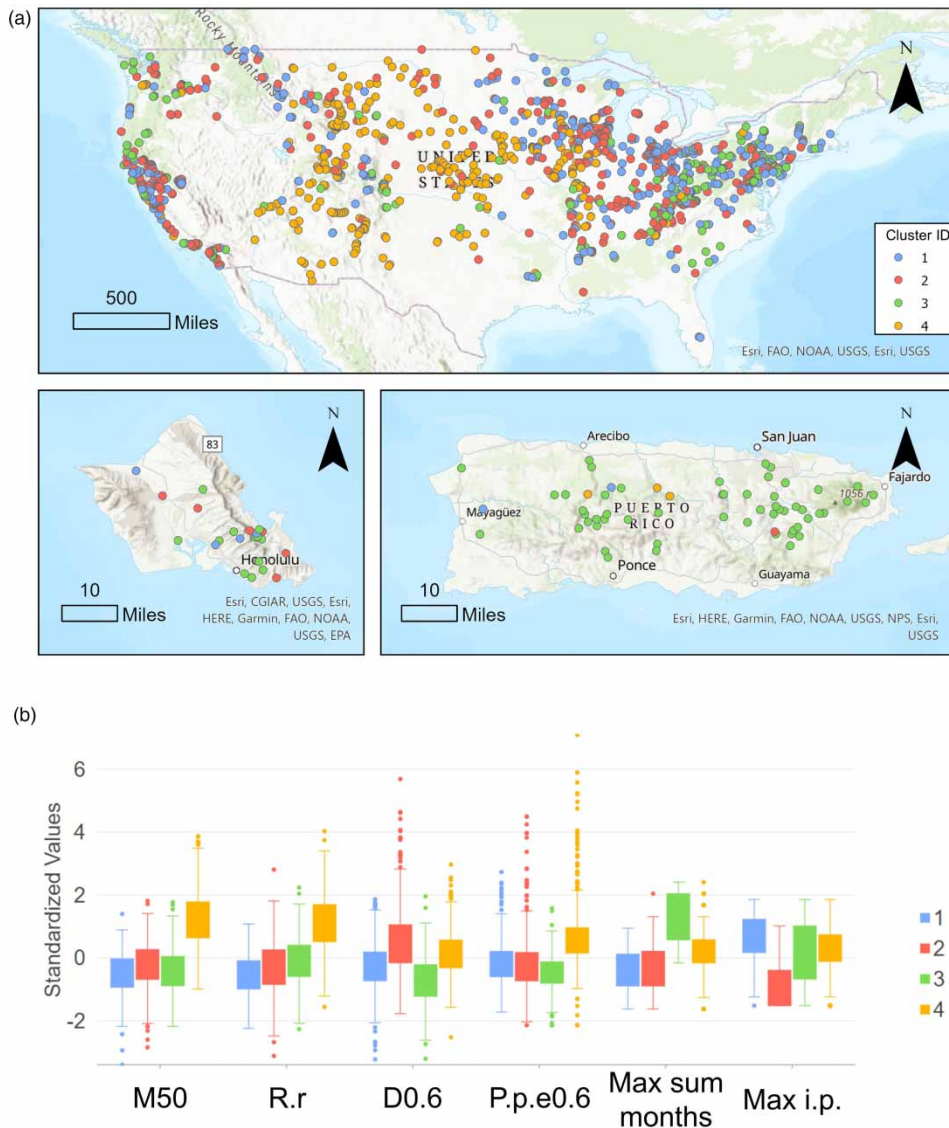


Figure 9 | Clustering of MFT: Variables consist of log transformed median SSC (M50), rising rate (R.r.), event duration at $\alpha = 0.6$ (D0.6), peaks per event at $\alpha = 0.6$ (P.p.e0.6) and months of maximum SSC (max sum months) and max number of SSC events (max i.p.) without transformation, showing the spatial distribution of the clusters in the continental US (a) and the relative differences between clusters for each indicator (b). Please refer to the online version of this paper to see this figure in colour: <http://dx.doi.org/10.2166/nh.2023.068>.

Midwest (Figure 6(e)), which may be due to short-duration intense precipitation in the summer (Alexandrov *et al.* 2007). Again, the strong covariation between the duration indicators suggests that a single indicator (e.g. D0.6) may be appropriate for further research (Figure 3).

The spatial pattern of the timing of SSC events suggests a strong climatic signal for magnitude but not frequency. The highest SSC values were found to occur almost exclusively in winter (DJF) in the west coast region of the US and in autumn in Puerto Rico (Figure 7(a); purple). These results correlate to periods of high rainfall and availability of erodible materials (Guirguis *et al.* 2019), for example, the late summer and autumn Atlantic hurricane season for Puerto Rico. The majority of sites across the US had their highest SSC in spring and summer, but there was no clear spatial pattern, suggesting influences of local factors that affect sediment availability (LULC) overlain onto climatic patterns. For example, the sites with summer (JJA, blue) could be caused by higher and more intense rainfall in this period, while the spring sites might be influenced by agricultural management practices (e.g. ploughing and sowing). While some clusters of high frequency SSC events

are apparent (e.g. upper Midwest in summer) that may relate to climate (e.g. convective storms), more research is needed to determine the utility of this indicator (Figure 7(b)).

The trend analysis identified largely decreasing trends in magnitude (Figure 8(a) and 8(c)) in accordance with the overall decreasing trend of SSC (Li *et al.* 2020b), which is believed to be due to SS management, e.g. soil conservation (Paolo & Minella 2020). However, increasing trends were identified for duration and frequency indicators over large areas of the country (Figure 8(d)–8(f)). Thus, while SSC magnitude is decreasing, periods of elevated SSC (relative to the annual average) are lasting longer in rivers. These results align with a hypothesis that improved soil management is decreasing rainfall-induced erosion and transport to river channels, resulting in a less anthropogenically influenced, flashy SS regime. The localised areas of increasing magnitude might be due to changes of land uses (Murphy 2020). However, due to the limitations and uncertainties in the daily SSC dataset (Sommerfield 2016), interpretation of new indicators about trend analysis requires consideration of uncertainty.

The spatial patterns for MFT indicators were integrated in the cluster analysis, which, despite considerable heterogeneity, showed some important large-scale spatial patterns (Figure 9). Sites in the Great Plains, central Rocky Mountain, and North American Desert regions were associated with the highest M50, R.r. and P.p.e 0.6, which may be associated with LULC and availability of erodible materials, perhaps due to agriculture. Sites with a low M50 and low R.r. with the greatest number of SSC events in summer (i.e. a high month of max i.p. in the hydrological year) were found across the Midwest, Appalachian and northern Rocky Mountain regions. Sites with a moderate M50 and R.r., low D0.6, and a timing of highest SSC in autumn (green) were identified across the US, but a pronounced cluster was found in the Appalachian region, northern California and in pockets on the west coast. The spatial patterns are likely due to a mixture of human impacts and LULC, e.g. higher impacts of magnitude in the driest and mountainous regions, longer duration of events from urban areas, and P.p.e. from areas where receives frequent precipitation events (Li *et al.* 2020b; Tazsarek *et al.* 2020). For future studies we recommend the use of a combination of magnitude (e.g. M50 or M95, R.r.), frequency (e.g. D0.6 and/or P.p.e 0.6) and timing (e.g. Max sum months and Max i.p.), especially when climate is a factor.

CONCLUSIONS

New indicators of SS transport dynamics were used to characterise the MFT of SS transport dynamics. Large-scale patterns in magnitude and frequency indicators were identified, which could be caused by climate and land use. Sites with the highest SSC events (M95) were located in the desert and mountainous regions, while sites with the longest duration of SSC events were found in the upper Midwest. Timing indicators showed varying patterns with clear dominant seasons for higher SSC in the western US and Puerto Rico but a high spatial heterogeneity for the season with the most events (Max i.p.). The trend analysis confirmed the decreasing trend in SSC magnitude reported by other studies but provides new evidence of increasing trends for the duration of SSC events and the number of P.p.e. These indicators provide new insights into the spatial variability of temporal dynamics in SSC in rivers and can be used by studies to determine the catchment and climatic controls. We recommend the use of an MFT indicator for future studies, particularly $\alpha = 0.6$ to capture short-term dynamics, which may be useful coupled with M95 and R.r. for climate change impact studies. A deeper understanding of the drivers of SSC dynamics will support the prediction of climate change impacts on SSC and develop mitigation measures to reduce the ecological and societal impacts of SS transport.

ACKNOWLEDGEMENTS

The authors would like to thank the anonymous reviewers for their careful and thoughtful review of earlier versions of the manuscript. The first author acknowledges bursary support from Cranfield University for this research.

DATA AVAILABILITY STATEMENT

The original data were obtained freely from USGS water data portal (<https://waterdata.usgs.gov/nwis>). The processed data used in the analyses are available at CORD data repository (10.17862/cranfield.rd.22233829).

CONFLICT OF INTEREST

The authors declare there is no conflict.

REFERENCES

- Akinsanola, A., Kooperman, K., Pendergrass, P., Hannah, H. & Reed, R. 2020 Seasonal representation of extreme precipitation indices over the United States in CMIP6 present-day simulations. *Environmental Research Letters* **15** (9). doi: 10.1088/1748-9326/ab92c1.
- Alexandrov, Y., Laronne, J. B. & Reid, I. 2007 Intra-event and inter-seasonal behaviour of suspended sediment in flash floods of the semi-arid northern Negev, Israel. *Geomorphology* **85** (1–2), 85–97. doi: 10.1016/j.geomorph.2006.03.013.
- Ballabio, C., Borrelli, P., Spinoni, J., Meusburger, K., Michaelides, S., Beguería, S., Klik, A., Jane, M., Olsen, P., Aalto, J., Lakatos, M., Rymaszewicz, A., Dumitrescu, A., Per, M., Diodato, N., Kostalova, J., Rousseva, S., Banasik, K., Alewell, C. & Panagos, P. 2017 'Mapping monthly rainfall erosivity in Europe'. *Science of the Total Environment* **579** (September 2016), 1298–1315. doi:10.1016/j.scitotenv.2016.11.123.
- Bilotta, G. S. & Brazier, R. E. 2008 Understanding the influence of suspended solids on water quality and aquatic biota. *Water Research* **42** (12), 2849–2861. doi: 10.1016/j.watres.2008.03.018.
- Celestino, A. E. M., Cruz, D. A. M., Sánchez, E. M. O., Reyes, F. G. & Soto, D. V. 2018 Groundwater quality assessment: an improved approach to K-means clustering, principal component analysis and spatial analysis: a case study. *Water (Switzerland)* **10** (4), 1–21. doi:10.3390/w10040437.
- Cohen, S., Syvitski, J., Ashley, T., Lammers, R., Fekete, B. & Li, H. 2022 Spatial trends and drivers of bedload and suspended sediment fluxes in Global Rivers. *Water Resources Research* 1–21. doi: 10.1029/2021WR031583.
- Edwards, T. K. & Douglas Glysson, G. 1999 *Field Methods for Measurement of Fluvial Sediment', Techniques of Water-Resources Investigations of the U.S. Geological Survey, Book 3, Ap (Chapter C2 Field Methods for Measurement of Fluvial Sediment)*. U.S. Geological Survey, Reston, VA.
- Fang, Y., Chen, H., Lin, Y., Zhao, C., Lin, Y. & Zhou, F. 2021 Classification of Northeast China cold vortex activity paths in early summer based on K-means clustering and their climate impact. *Advances in Atmospheric Sciences* **38** (3), 400–412. doi: 10.1007/s00376-020-0118-3.
- Francke, T., Werb, S., Sommerer, E. & López-Tarazón, J. A. 2014 Analysis of runoff, sediment dynamics and sediment yield of subcatchments in the highly erodible Isábena catchment, Central Pyrenees. *Journal of Soils and Sediments* **14** (12), 1909–1920. doi: 10.1007/s11368-014-0990-5.
- Girolamo, A. M. D., Pappagallo, G. & Porto, A. L. 2015 Temporal variability of suspended sediment transport and rating curves in a Mediterranean river basin : the Celone (SE Italy). *Catena* **128**, 135–143. Elsevier B.V.. doi: 10.1016/j.catena.2014.09.020.
- Guirguis, K., Gershunov, A., Shulgina, T., Clemesha, R. E. S. & Ralph, F. M. 2019 Atmospheric rivers impacting Northern California and their modulation by a variable climate. *Climate Dynamics* **52** (11), 6569–6583. Springer Berlin Heidelberg. doi: 10.1007/s00382-018-4532-5.
- Hegde, V. 2016 Dimensionality reduction technique for developing undergraduate student dropout model using principal component analysis through R package. In: *2016 IEEE International Conference on Computational Intelligence and Computing Research (ICIC)*. IEEE, pp. 1–6. doi:10.1109/ICIC.2016.7919670.
- Hoess, R. & Geist, J. 2021 Effect of fish pond drainage on turbidity, suspended solids, fine sediment deposition and nutrient concentration in receiving pearl mussel streams *. *Environmental Pollution* **274**, 116520. Elsevier Ltd.. doi: 10.1016/j.envpol.2021.116520.
- Horowitz, A. J. 2003 An evaluation of sediment rating curves for estimating suspended sediment concentrations for subsequent flux calculations. **3409** (January), 3387–3409. doi: 10.1002/hyp.1299.
- Kar, R. & Sarkar, A. 2021 Anthropogenic influences on the variation of runoff and sediment load of the Mahanadi River Basin. *Hydrological Sciences Journal* **66** (12), 1820–1844. Taylor & Francis. doi:10.1080/02626667.2021.1967957.
- Kemper, J. T., Miller, A. J. & Welty, C. 2019 Spatial and temporal patterns of suspended sediment transport in nested urban watersheds. *Geomorphology* **336**, 95–106. Elsevier B.V.. doi:10.1016/j.geomorph.2019.03.018.
- Khan, M. Y. A., Daityari, S. & Chakrapani, G. J. 2016 Factors responsible for temporal and spatial variations in water and sediment discharge in Ramganga River, Ganga Basin, India. *Environmental Earth Sciences* **75** (4), 1–18. doi: 10.1007/s12665-015-5148-2.
- Ladson, A. R., Brown, R., Neal, B. & Nathan, R. 2013 A standard approach to baseflow separation using the Lyne and Hollick filter. *Australian Journal of Water Resources* **17** (1), 25–34. doi: 10.7158/W12-028.2013.17.1.
- Ladson, A. R., Brown, R., Neal, B., Nathan, R. & Merz, S. K. 2015 A standard approach to baseflow separation using the Lyne and Hollick Filter A standard approach to baseflow separation using the Lyne and Hollick filter *. **1583**. doi: 10.7158/13241583.2013.11465417.
- Li, L., Ni, J., Chang, F., Yue, Y., Frolova, N., Magritsky, D., Borthwick, A. G. L., Ciais, P., Wang, Y., Zheng, C. & Walling, D. E. 2020a Global trends in water and sediment fluxes of the world's large rivers. *Science Bulletin* **65** (1), 62–69. doi: 10.1016/j.scib.2019.09.012.
- Li, T., Wang, S., Liu, Y., Fu, B. & Zhao, W. 2020b A retrospective analysis on changes in sediment flux in the Mississippi River system: trends, driving forces, and implications. *Journal of Soils and Sediments* **26** (7), 1719–1729.
- Liu, J., Sleeter, B. M., Zhu, Z., Loveland, T. R., Sohl, T., Howard, S. M., Key, C. H., Hawbaker, T., Liu, S., Reed, B., Cochrane, M. A., Heath, L. S., Jiang, H., Price, D. T., Chen, J. M., Zhou, D., Bliss, N. B., Wilson, T., Sherba, J., Zhu, Q., Luo, Y. & Poulter, B. 2020 Critical land change information enhances the understanding of carbon balance in the United States. *Global Change Biology* **26** (7), 3920–3929. doi: 10.1111/gcb.15079.
- Masud, A., Zhexue, J., Wei, C. & Wang, J. 2018 I-nice : a new approach for identifying the number of clusters and initial cluster centres. **466**, 129–151. Elsevier Inc. doi:10.1016/j.ins.2018.07.034.
- Misset, C., Recking, A., Legout, C., Poirel, A., Cazilhac, M., Esteves, M. & Bertrand, M. 2019 An attempt to link suspended load hysteresis patterns and sediment sources configuration in alpine catchments. *Journal of Hydrology* **576** (November 2018), 72–84. Elsevier. doi:10.1016/j.jhydrol.2019.06.039.

- Mize, S. V., Murphy, J. C., Diehl, T. H. & Demcheck, D. K. 2018 Suspended-sediment concentrations and loads in the lower Mississippi and Atchafalaya rivers decreased by half between 1980 and 2015. *Journal of Hydrology* **564** (May), 1–11. Elsevier. doi:10.1016/j.jhydrol.2018.05.068.
- Moragoda, N. & Cohen, S. 2020 Climate-induced trends in global riverine water discharge and suspended sediment dynamics in the 21st century. *Global and Planetary Change* **191** (September 2019), 103199. Elsevier. doi: 10.1016/j.gloplacha.2020.103199.
- Murphy, J. C. 2020 Changing suspended sediment in United States rivers and streams: linking sediment trends to changes in land use/cover, hydrology and climate. *Hydrology and Earth System Sciences* **24** (2), 991–1010. doi: 10.5194/hess-24-991-2020.
- Neachell, E. 2014 Book review – environmental flows: saving rivers in the third millennium. *River Research and Applications* **30** (January), 132–133. doi: 10.1002/rra.
- Nosrati, K., Mohammadi-raigani, Z., Haddadchi, A. & Collins, A. L. 2021 Elucidating intra-storm variations in suspended sediment sources using a Bayesian fingerprinting approach. *Journal of Hydrology* **596** (December 2019), 126115. Elsevier B.V.. doi: 10.1016/j.jhydrol.2021.126115.
- Paolo, J. & Minella, G. 2020 Monitoring sediment yield for soil and water conservation planning in rural catchments. *Environmental Monitoring and Assessment* **192**, 1–19.
- Plexida, S. G., Sfougaris, A. I., Ispikoudis, I. P. & Papanastasis, V. P. 2014 Selecting landscape metrics as indicators of spatial heterogeneity–A comparison among Greek landscapes. *International Journal of Applied Earth Observation and Geoinformation* **26** (1), 26–35. Elsevier B.V.. doi: 10.1016/j.jag.2013.05.001.
- Poeppel, R. E., Coulthard, T., Keesstra, S. D. & Keiler, M. 2019 Modeling the impact of dam removal on channel evolution and sediment delivery in a multiple dam setting. *International Journal of Sediment Research* **34** (6), 537–549. Elsevier Ltd. doi: 10.1016/j.ijsrc.2019.06.001.
- Porterfield, G. 1972 *Computation of Fluvial-Sediment Discharge. U.S. Geological Survey Techniques of Water-Resource Investigations, Book 3, Chapter C3*. USGS, Arlington, VA, p. 66.
- Posit team. 2022 *RStudio: Integrated Development Environment for R. Posit Software*. PBC, Boston, MA. Available from: <http://www.posit.co/>.
- Roman, D. C., Vogel, R. M. & Schwarz, G. E. 2012 Regional regression models of watershed suspended-sediment discharge for the eastern United States. *Journal of Hydrology* **472–473**, 53–62. Elsevier B.V.. doi: 10.1016/j.jhydrol.2012.09.011.
- Rose, L. A. & Karwan, D. L. 2021 Stormflow concentration – discharge dynamics of suspended sediment and dissolved phosphorus in an agricultural watershed. (December), 1–16. doi:10.1002/hyp.14455.
- Shin, J., Grabowski, R. C. & Holman, I. P. In: Revision Catchment and climatic influences on spatio-temporal variations in suspended sediment transport dynamics in rivers. *Hydrology Research*. (Manuscript Reference No: Hydrology-D-22-00127R1)
- Sommerfield, C. K. 2016 Qualities and limitations of fluvial suspended sediment data published by the United States geological survey. *Journal of Coastal Research* **32** (5), 719–724. doi: 10.2112/JCOASTRES-D-15-00143.1.
- Stryker, J., Wemple, B. & Bomblies, A. 2018 Journal of hydrology: regional studies modeling the impacts of changing climatic extremes on stream flow and sediment yield in a northeastern US watershed. *Journal of Hydrology: Regional Studies* **17** (February), 83–94. Elsevier. doi: 10.1016/j.ejrh.2018.04.003.
- Taszarek, M., Allen, J. T., Groenemeijer, P., Edwards, R., Brooks, H. E., Chmielewski, V. & Enno, S. E. 2020 Severe convective storms across Europe and the United States. Part I: Climatology of lightning, large hail, severe wind, and tornadoes. *Journal of Climate* **33** (23), 10239–10261. doi: 10.1175/JCLI-D-20-0345.1.
- Tomlinson, D. A., Molik, D. C., Pfrender, M. E. & Emrich, S. J. 2018 The effects of normalization, transformation, and rarefaction on clustering of OTU abundance. In: *2018 IEEE International Conference on Bioinformatics and Biomedicine (BIBM)*. Madrid, Spain, 3-6 December 2018. IEEE, New York, pp. 2810–2812. doi: 10.1109/BIBM.2018.8621347.
- Tsyplenkov, A., Vanmaercke, M., Collins, A. L., Kharchenko, S. & Golosov, V. 2021 Elucidating suspended sediment dynamics in a glacierized catchment after an exceptional erosion event : the Djankuat catchment, Caucasus. *Catena* **203** (March), 105285. Elsevier B. V.. doi: 10.1016/j.catena.2021.105285.
- Uhrich, M. A., Spicer, K. R., Mosbrucker, A. R., Saunders, D. R. & Christianson, T. S. 2021 A 40-year story of river sediment at Mount St. Helens: U.S. Geological Survey Fact Sheet 2021–3004, 6 p., <https://doi.org/10.3133/fs20213004>.
- U.S. Geological Survey 2016 *National Water Information System Data Available on the World Wide Web (USGS Water Data for the Nation)*. Available from: <http://waterdata.usgs.gov/nwis/> (accessed 15 October 2021).
- Vercruyse, K., Grabowski, R. C. & Rickson, R. J. 2017 Suspended sediment transport dynamics in rivers: multi-scale drivers of temporal variation. *Earth-Science Reviews* **166**, 38–52. Elsevier B.V.. doi: 10.1016/j.earscirev.2016.12.016.
- Wang, K. & Steinschneider, S. 2022 Characterization of multi-scale fluvial suspended sediment transport dynamics across the United States using turbidity and dynamic regression. *Water Resources Research* **58** (10). doi: 10.1029/2021WR031863.
- Wharton, G., Mohajeri, S. H. & Righetti, M. 2017 The pernicious problem of streambed colmation: a multi-disciplinary reflection on the mechanisms, causes, impacts, and management challenges. *Wiley Interdisciplinary Reviews: Water* **4** (5), 1–17. doi: 10.1002/WAT2.1231.
- Whitfield, P. H. & Shook, K. R. 2020 Changes to rainfall, snowfall, and runoff events during the autumn – winter transition in the Rocky Mountains of North America transition in the Rocky Mountains of North America. *Canadian Water Resources Journal/Revue canadienne des Ressources Hydriques* **45** (1), 28–42. Taylor & Francis. doi: 10.1080/07011784.2019.1685910.
- Yang, M., Gao, X., Zhao, X. & Wu, P. 2021 Scale effect and spatially explicit drivers of interactions between ecosystem services – A case study from the Loess Plateau. *Science of the Total Environment* **785** (26), 147389. Elsevier B.V.. doi: 10.1016/j.scitotenv.2021.147389.

- Yao, Q., Joshi, S., Liu, K. B., Rodrigues, E. & Yin, D. 2022 A multi-decadal analysis of river discharge and suspended sediment load in three Texas coastal rivers in relation to hurricanes, seasonal rainfall, and ENSO. *Frontiers in Earth Science* **10** (September), 1–17. doi: 10.3389/feart.2022.886614.
- Yilmaz, B., Aras, E., Nacar, S. & Kankal, M. 2018 Estimating suspended sediment load with multivariate adaptive regression spline, teaching-learning based optimization, and artificial bee colony models. *Science of the Total Environment* **639**, 826–840. Elsevier B.V.. doi: 10.1016/j.scitotenv.2018.05.153.
- Yu, G. A. & Disse, M. 2017 Sediment dynamics of an allogenic river channel in a very arid environment. (March), 2050–2061. doi: 10.1002/hyp.11171.

First received 17 May 2023; accepted in revised form 13 July 2023. Available online 21 July 2023